

Novel Sol–Gel Precursors for Thin Mesoporous Eu³⁺-Doped Silica Coatings as Efficient Luminescent Materials.

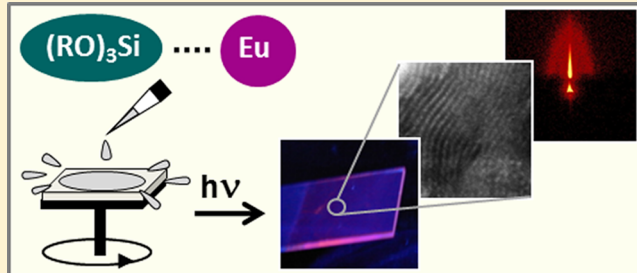
Andrea Feinle,[†] Flavie Lavoie-Cardinal,[‡] Johanna Akbarzadeh,[§] Herwig Peterlik,[§] Matthias Adlung,[‡] Claudia Wickleder,^{*,‡} and Nicola Hüsing^{*,†}

[†]Materials Chemistry, Paris–Lodron University Salzburg, Hellbrunner Str. 34, A-5020 Salzburg, Austria

[‡]Inorganic Chemistry II, University of Siegen, D-57068 Siegen, Germany

[§]Faculty of Physics, University of Vienna, Strudlhofgasse 4, A-1090 Vienna, Austria

ABSTRACT: Europium(III) ions containing mesoporous silica coatings have been prepared via a solvent evaporation-induced self-assembly (EISA) approach of different single-source precursors (SSPs) in the presence of Pluronic P123 as a structure-directing agent, using the spin-coating process. A deliberate tailoring of the chemical composition of the porous coatings with various Si:Eu ratios was achieved by processing mixtures of tetraethylorthosilicate (TEOS) and Eu³⁺-coordinated SSPs. Small-angle X-ray scattering (SAXS) and transmission electron microscopy (TEM) analyses demonstrate that the thin metal oxide-doped silica coatings consist of a porous network with a short-range order of the pore structure, even at high europium(III) loadings. Furthermore, luminescence properties were investigated at different temperatures and different degrees of Eu³⁺ contents. The photoluminescence spectra clearly show characteristic emission peaks corresponding to the $^5D_0 \rightarrow ^7F_J$ ($J = 0-5$) transitions resulting in a red luminescence visible by the eyes, although the films have a very low thickness (150–200 nm).



KEYWORDS: *thin films, luminescence, SiO₂/Eu₂O₃, single-source precursor, sol gel process*

1. INTRODUCTION

Solid luminescent materials have attracted much attention during the last decades, because of their wide range of applications in our daily life such as in lamps, sensors, X-ray detectors, and fluorescent tubes.^{1,2} One strong research focus is on the improvement of the quantum yields or the spectral energy distribution, and with their narrow emission peaks, rare-earth luminescent materials soon became important in this area.^{3,4} New fields of applications (e.g., novel laser materials, luminescent markers in biological devices, or light-emitting diodes (LEDs)),^{2,5,6} have been established and there still has been a lot of effort devoted to the further development of new lanthanide-doped materials with improved chemical stability. For this goal, the lanthanide ions must be inserted into a stable inorganic, organic, or inorganic–organic hybrid matrix.⁷ Particularly, the incorporation of lanthanide ions into inorganic mesoporous hosts with high specific surface areas has attracted much interest in recent years (e.g., for catalytic devices, adsorbents, and separation agents and in the development of optical sensors).^{7–10}

An applicable method for the preparation of such materials is based on sol–gel processing, in which the low temperatures allow the introduction of coordination compounds and organic moieties.^{1,11–13} With its sharp, near-monochromatic emission line centered at ~611 nm and the resulting outstanding luminescence properties,^{14,15} europium(III)-doped mesoporous

silica materials are of special interest and several synthetic routes toward these materials using the sol–gel process have been reported. This can be a one-step synthesis by mixing Eu₂O₃ nanoparticles in a spin-coating solution,¹⁶ a post-synthetic grafting of MCM-41 materials with europium(III) β-diketonate complexes,^{7,17} or the often used co-condensation method of two different precursors (for example, tetraethylorthosilicate (TEOS) and europium(III) nitrate).¹⁴ However, one must consider that the luminescence efficiency of europium(III) ions embedded in a silica matrix is limited by the aggregation of the rare-earth metal at higher concentrations or by hydroxyl groups of residual water and unreacted silanol groups, both leading to a remarkable quenching of the emission.¹⁸ Therefore, it is indispensable that the europium(III) ions are homogeneously dispersed in the silica matrix. This can hardly be realized by the co-condensation method, because the reaction rates of the molecular precursors differ greatly and, as a result, no homogeneous dispersion is achieved, but phase separation can occur easily.¹⁹ To overcome this inherent problem, it is necessary to adjust the reaction rates of the individual components by (i) prehydrolyzing the slower reacting component,^{20,21} (ii) chemical modification of the faster

Received: March 30, 2012

Revised: August 29, 2012

Published: August 29, 2012

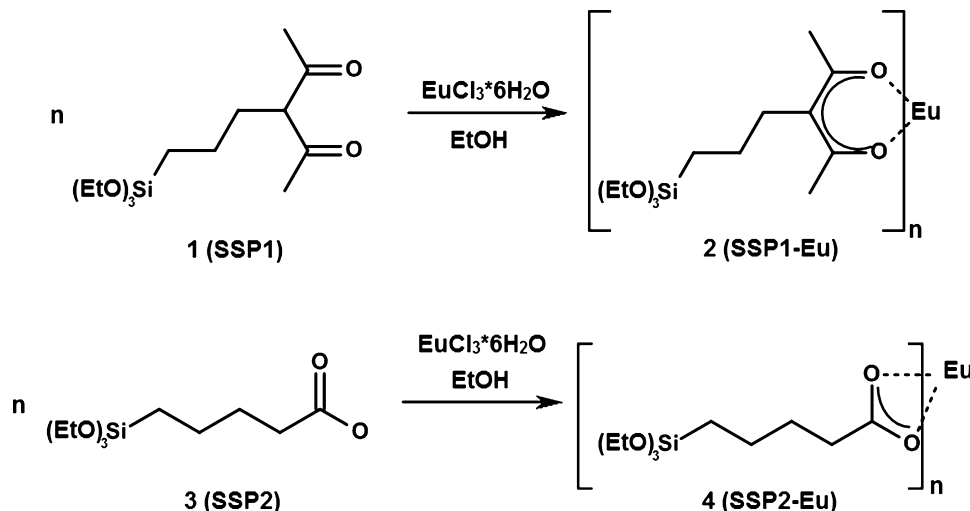


Figure 1. Synthesis of metal-coordinated (Eu^{3+}) single-source precursor molecules ($n = 1-3$).

reacting component,²² or (iii) the application of single-source precursors (SSPs), in which the matrix-forming silane and the active rare-earth metal species are coordinatively linked via an organic spacer.

In the present work, we report the coordination of europium(III) ions to two tailor-made functional silanes (see Figure 1), carrying coordinating organic moieties and the application of these two different SSPs in the preparation of europium(III)-doped mixed oxide coatings. Special emphasis is given to the investigation of the influence of an increasing amount of europium(III) on the structural and luminescence properties of the final coatings.

2. EXPERIMENTAL SECTION

2.1. Materials. Ethanol (96%), acetone (99%), potassium carbonate (99%), sodium iodide (99%), tetraethoxysilane (99.9%), and hydrochloric acid were purchased from Merck KGaA (Darmstadt, Germany). 3-(Chloropropyl)triethoxysilane (97%), acetylacetone (99%), the nonionic surfactant poly(ethylene glycol)-block-poly(propylene glycol)-block-poly(ethylene glycol) (Pluronic P123TM) and europium(III)-chloride hexahydrate (99%) were supplied by Sigma-Aldrich (Munich, Germany) and used as received. Glass substrates ($d = 18$ mm) were supplied by Menzel (Braunschweig, Germany) and *p*-doped silicon wafers with (100) orientation were supplied by Active Business Company GmbH (Brunnthal, Germany). Acetone was dried over a molecular sieve of 3 Å. All other chemicals were used without further purification.

2.2. Synthesis of the Organosilanes. The acetylacetone-modified precursor SSP1 was synthesized according to Schubert et al.^{23,24}

3-(Chloropropyl)triethoxysilane was added to a suspension of sodium iodide in acetone under an argon atmosphere. After heating under reflux overnight, potassium carbonate and acetylacetone were added and heated under reflux again. After cooling to room temperature, the mixture was centrifuged and the solvent was distilled off. The resulting crude product was purified via distillation under reduced pressure. The organosilane SSP2 was synthesized according to a literature procedure.²⁵

2.3. Synthesis of the Precursor Solutions. Three weight percent (3 wt %) of the surfactant Pluronic P123 were dissolved in a mixture of 0.16 mol ethanol, 24.98 mmol

distilled water, and 9.04 mmol hydrochloric acid as a catalyst and tetraethylorthosilicate (TEOS). This mixture was stirred for 1 h in a closed polypropylene bottle to prehydrolyze the slower reacting silica precursor. In case of pure silica precursor solutions, the synthesized organosilane SSP1 or SSP2 was added directly to the prehydrolyzed solution, whereas the single-source precursor had to be previously synthesized. Therefore, the organosilane SSP1 or SSP2 was added to an ethanolic solution of $\text{EuCl}_3 \cdot 6\text{H}_2\text{O}$ in a molar ratio of 3:1 or 1:1 (organosilane:Eu), respectively. After this *in situ* synthesis, the single-source precursor was added to the prehydrolyzed TEOS solution and the sol was aged for another hour prior to the coating process. Different organosilane or europium(III) concentrations in the precursor solutions were adjusted by variable amounts of the individual precursors. For the pure silica coatings prepared with TEOS and an organosilane SSP1 or SSP2, TEOS is directly replaced by the same molar amount of the organosilane, because both precursors exhibit one hydrolyzable silicon center. In contrast, if TEOS is replaced by one of the metal-coordinated SSPs, in which the ratio of organosilane to europium(III) is 3:1, it must be considered that the SSP now contains four hydrolyzable centers. That means that, in the case of a coating with, e.g., 2.5 mol % SSP1-Eu (2.5 mol %, according to 8.40 mmol hydrolyzable metal centers), 7.56 mmol TEOS and 0.21 mmol SSP1-Eu are needed. Accordingly, for the sample with 12.5 mol % SSP1-Eu, 4.20 mmol TEOS and 1.05 mmol SSP1-Eu were used, and for the coating with 25 mol % SSP1-Eu, 0 mmol TEOS and 2.1 mmol SSP1-Eu were used (see Table 1).

2.4. Synthesis of $\text{SiO}_2/\text{Eu}_2\text{O}_3$ Mixed-Oxide Coatings. Europium(III) oxide-doped silica coatings were prepared on commercially available glass slides and silicon wafers with (100) orientation by spin coating (rotation speed of 4000 rpm). The substrates were ultrasonically cleaned with ethanol for 15 min prior to use. After the coating process the samples were first aged overnight at room temperature and afterward at 120 °C for 10 h. Finally, the coatings were calcined in air at 350 °C for 3 h with a heating ramp rate of 1 °C min⁻¹.

For the nitrogen sorption measurements, a larger quantity of the mixed-oxide material was needed. The remaining coating solution was cast in Petri dishes and analogously aged to the thin coatings. After the aging step, the material was scraped off and calcined in air for 3 h at 550 °C with a heating ramp rate of

Table 1. Molar Amounts of Tetraethylorthosilicate (TEOS) and the Single-Source Precursor Used for the Synthesis of the Coatings

ligand:Eu ³⁺ ratio	coating assignment	<i>n</i> (TEOS)	<i>n</i> (SSPX-Eu)s
3:1	2.5 mol % SSP1-Eu	7.56 mmol	0.21 mmol SSP1-Eu
3:1	12.5 mol % SSP1-Eu	4.20 mmol	1.05 mmol SSP1-Eu
3:1	25.0 mol % SSP1-Eu	0 mmol	2.10 mmol SSP1-Eu
3:1	2.5 mol % SSP2-Eu	7.56 mmol	0.21 mmol SSP2-Eu
3:1	12.5 mol % SSP2-Eu	4.20 mmol	1.05 mmol SSP2-Eu
3:1	25.0 mol % SSP2-Eu	0 mmol	2.10 mmol SSP2-Eu
1:1	50.0 mol % SSP2-Eu	0 mmol	4.20 mmol SSP2-Eu

1 °C min⁻¹. One must keep in mind that the data obtained from nitrogen sorption measurements for scraped coatings might deviate from the data for the coatings on glass slides.

2.5. Characterization. For nitrogen sorption measurements, the calcined samples were degassed under vacuum at 300 °C for 3 h and measured on a NOVA 4000e (Quantachrome Instruments, USA) at 77 K in the relative pressure range of $p/p_0 = 0.05$ –0.99. For the calculation of the specific surface area (BET), the 5-point method in the relative pressure range from 0.05 to 0.30, according to Brunauer et al.,²⁶ was used.

Powder X-ray diffraction (XRD) patterns were recorded on a PANalytical MPD PRO diffractometer (PANalytical, The Netherlands) using Cu K α radiation.

The elemental composition of the coatings was determined by X-ray photoelectron spectroscopy (XPS) measured on a PHI 5800 ESCA System (Physical Electronics) using monochromatic Al K α radiation. Transmission electron microscopy (TEM) images were obtained using a Philips EM 400 (Philips, The Netherlands; $U = 80$ kV). Small-angle X-ray scattering (SAXS) and grazing-incidence small-angle X-ray scattering (GISAXS) measurements of the coated films were performed under vacuum with a rotating-anode X-ray generator equipped with a pinhole camera (Nanostar, Bruker AXS). Cu K α radiation was monochromatized and collimated from crossed Goebel mirrors, and the scattered intensity was detected by a two-dimensional (2D) position-sensitive detector (Vantec 2000). The sample-to-detector distance was 108 cm, from which scattering data in the q -range from 0.1 to 2.8 nm⁻¹ were obtained.

The SAXS patterns were radially averaged and corrected for background scattering to obtain the scattering intensities in dependence on the scattering vector $q = 4\pi/\lambda \sin \theta$, where 2θ is the scattering angle and λ is the X-ray wavelength ($\lambda = 0.1542$ nm). In order to quantify the SAXS data, the background scattering was subtracted using a linear baseline, and the diffraction peaks were fitted with a Lorentzian function. The d -spacing was calculated from the peak maximum (in the case of a perfect hexagonal lattice, the pore-to-pore distance would be $a = 2d/\sqrt{3}$, with $d = 2\pi/q_{\max}$). The size of the hexagonal domains was calculated using the Scherrer equation. This size is interpreted here as the crystallite size, but represents only a lower limit, because polydispersity (statistical variation of cylinder diameter) and translational disorder (statistical variation of the cylinder centers)²⁷ also might contribute to the peak broadening. Since we have a 2D lattice, we use the formula for 2D particles (the value being twice as large as the corresponding value for three-dimensional (3D) particles²⁸), $l_a = (2\pi K)/\Delta q$.²⁹ This equation is the form of the reciprocal,³⁰

not the angular space.²⁸ Here, Δq is the full width at half-maximum (FWHM) of the peak intensity and K is the Scherrer constant (a number close to 1, 0.94 for crystallite cubes).

The film thickness was detected by a DEKTAK 150 surface profiler (Veeco Instrument, Inc., USA) with a 2.5-μm tip and a tipping force of 10 mg.

Photoluminescence emission and excitation, as well as lifetime measurements, were performed with the aid of a Fluorolog3 spectrofluorometer (Model Fl3-22, Horiba Jobin-Yvon) that was equipped with double Czerny-Turner monochromators, a 450-W xenon lamp, and a R928P photomultiplier with a photon counting system. Cooling down to 10 K was achieved by a closed-cycle He cryostat (Janis Research). All emission spectra were corrected for the photomultiplier sensitivity, and all excitation spectra were corrected for the intensity of the excitation source.

3. RESULTS AND DISCUSSION

3.1. Synthesis and Structural Properties. Several authors describe the preparation of sol-gel-based mixed-oxide materials via approaches such as the direct synthesis starting from different precursors (e.g., tetramethoxysilane (TMOS) and Eu(NO₃)₃·H₂O),³¹ post-treatment of a pre-formed porous matrix (such as MCM-48 silica hosts, with europium(III) dibenzoylmethane complexes),³² or the coordination of the faster-reacting metal alkoxides to the structure-directing surfactant (e.g., Fe, Ti, Hf-mixed oxides).^{33–35}

In this study, a novel route to porous europium(III)-doped silica films is investigated using a prehydrolyzed silica sol and different europium(III)-coordinated organosilanes (see Figure 1). The acetylacetone-based organosilane SSP1 (1) has previously been applied for the synthesis of silica-titania mixed metal oxide materials with no long-range ordering of the pores via the complexation of tetraisobutylorthotitanate,³⁶ as well as for thin silica-titania coatings in biological applications.³⁷ In this work, we extend these reports to the complexation of europium(III). In addition, a second single-source precursor SSP2-Eu (4) was synthesized based on 5-(triethoxysilyl)pentanoic acid (3) and was also applied for the complexation of europium(III) ions and finally for the preparation of europium(III)-doped silica films.²⁵ These precursors now serve different functions. First of all, the rate of condensation of europium is controlled via the coordinative linkage to the organosilane, and second, based on the stable coordination, europium and silicon are positioned in close proximity to each other in the final material, thus phase separation in a silica-rich and europium oxide-rich phase is hindered. Based on the stability differences of the coordinative linkage and the number of coordinating molecules ($n = 1$ or $n = 3$), a different behavior in sol-gel processing as well as variations in the structural features of the coatings are expected, which will be investigated in detail in this work.

Based on a pure silica system using TEOS as silicon precursor and 3 wt % Pluronic P123 as a structure-directing agent,³⁸ TEOS was replaced step by step by a defined amount of the organosilane SSP1 (1) or SSP2 (3) and, furthermore, by the corresponding single-source precursor SSP1-Eu (2) or SSP2-Eu (4). For the pure silica systems, substitution of TEOS by the organosilane was calculated based on the number of silicon centers, i.e., 10 mol % of TEOS were substituted by 10 mol % of SSP1 or SSP2. For the europium(III)-coordinated SSP precursors, the calculation is based on the amount of hydrolyzable metal centers, thus including Si and Eu. The

amount of hydrolyzable centers was kept at a constant value of 0.0084 mol, meaning that, for $n = 1$, substitution of 10 mol % TEOS was done with 5 mol % of the SSP-Eu precursor, while for $n = 3$, substitution of 10 mol % TEOS resulted in 2.5 mol % of the SSP-Eu precursor. Table 2 gives the relationship between the amounts of the corresponding single-source precursor and the silicon-to-europium ratio of the final material.

Table 2. Relationship between the Applied Amounts of the SSP-Eu Precursor in mol % and the Composition of the Final Coatings. All Calculations are Based on the Amount of Hydrolysable Metal Centers of 8.40 mmol

n	TEOS		SSP-Eu		Si/Eu ratio
	mol %	n [mmol]	mol %	n [mmol]	
1	0		50.0	4.20	1/1
3	0		25.0	2.10	3/1
3	50.0	4.20	12.5	1.05	7/1
3	90.0	7.56	2.5	0.21	39/1

Via this approach, on the one hand, a direct comparison of the influence of an increasing amount of the pure organosilane on the properties of the final coating is possible, while, on the other hand, the influence of an europium(III) doping is also possible.

To investigate the structural properties of the coatings, small-angle X-ray scattering (SAXS) analyses in transmission geometry directly on the coating, as well as transmission electron microscopy (TEM) and nitrogen sorption measurements on the corresponding powders, were performed. The film thickness of the calcined coatings obtained for the different precursors (150 and 200 nm) are almost in the same range.

The SAXS intensities of pure silica films prepared with different TEOS/organosilane ratios after calcination at 350 °C are shown in Figure 2. Coatings prepared with TEOS as a sole precursor show a sharp peak at $q = 0.9 \text{ nm}^{-1}$, indicating large domains of hexagonally arranged mesopores ($l_a > 250 \text{ nm}$). The broader peak at $q = 0.7 \text{ nm}^{-1}$ for a coating containing 10 mol % SSP1 or 10 mol % SSP2 is due to the smaller size of the coherently scattering domains of hexagonally arranged mesopores ($l_a \approx 37 \text{ nm}$). The domain sizes l_a have been calculated from the FWHM using the Scherrer formula (also see Table 3).

This illustrates that the addition of increasing amounts of organosilanes, which can be described as trifunctional silicon precursors as well, lead to scattering curves without any observable peak and, consequently, to a complete destruction of the hexagonal ordering of the pores within the silica matrix.

The influence of an increasing amount of organosilane on the arrangement of the pore system in the mesoscopic range is clearly visible and has already been described in the literature.^{39–43} It can be attributed to several effects, such as a change in the polarity in the sol due to the organofunctional moiety, different reaction rates of the tetrafunctional to trifunctional silicon centers (tetrafunctional and trifunctional are given, with respect to the number of hydrolyzable groups). As a consequence, not only does heterocondensation between the different precursors take place, but also a possibility of homocondensation is given. In addition, with increasing amount of the organofunctional silane, the degree of condensation is reduced.

The SAXS measurements of the europium(III)-doped silica coatings prepared with the europium(III)-coordinated pre-

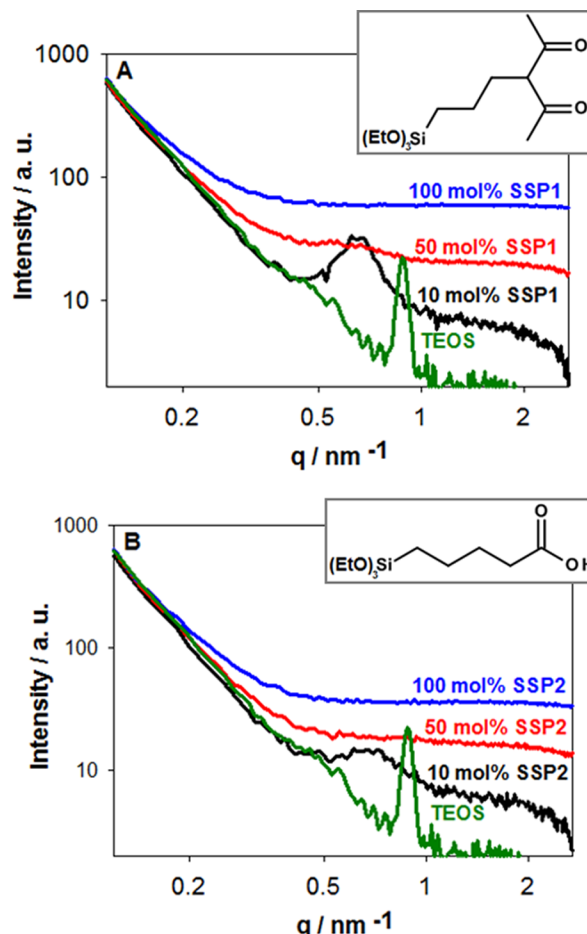


Figure 2. Small-angle X-ray scattering (SAXS) curves of pure silica coatings using different TEOS/organosilane ratios: (A) SSP1 and (B) SSP2.

Table 3. SAXS Data of the Various Coatings

sample	q_{\max} [nm^{-1}] ^a	d [nm] ^a	Δq [nm^{-1}]	l_a [nm] ^b
TEOS	0.88	7.2	0.05	240
10.0 mol % SSP1	0.66	9.52	0.17	37
50.0 mol % SSP1	0.63	9.96	0.45	28
100.0 mol % SSP1				
2.5 mol % SSP1-Eu (Si/Eu = 39/1)	0.65	9.71	0.15	84
12.5 mol % SSP1-Eu (Si/Eu = 7/1)	0.74	8.50	0.30	42
25.0 mol % SSP1-Eu (Si/Eu = 3/1)	0.48	13.1	0.15	84
10.0 mol % SSP2	0.71	8.85	0.33	38
50.0 mol % SSP2				
100.0 mol % SSP2				
2.5 mol % SSP2-Eu (Si/Eu = 39/1)	0.68	9.24	0.19	66
12.5 mol % SSP2-Eu (Si/Eu = 7/1)	0.54	11.64	0.13	97
25.0 mol % SSP2-Eu (Si/Eu = 3/1)	0.53	11.86	0.2	63

^a d -spacing. ^bSize of the hexagonal domains.

cursors SSP1-Eu and SSP2-Eu ($n = 3$) are compared in Figure 3. Although a significant broadening of the diffraction peak can be observed for an increasing amount of the single-source precursor, a low level of periodicity in the mesoscopic range,

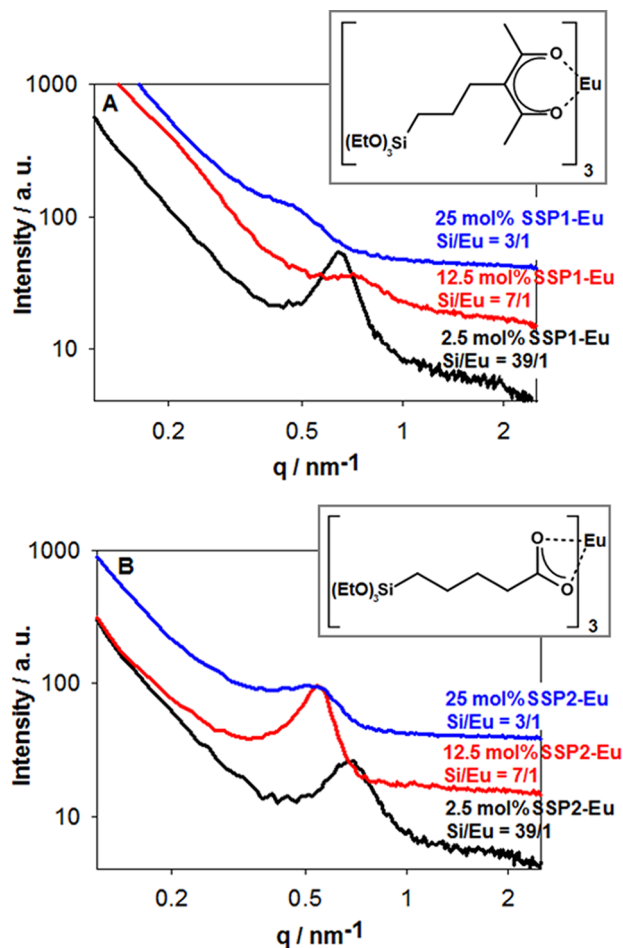


Figure 3. SAXS curves of europium(III)-doped silica coatings using TEOS and different amounts of the europium(III)-coordinated organosilane: (A) SSP1-Eu and (B) SSP2-Eu.

even at high europium(III) concentrations, is still observable (well pronounced for the SSP2-Eu coatings). Besides the broader diffraction peaks, a peak shift from $q = 0.68 \text{ nm}^{-1}$ to $q = 0.53 \text{ nm}^{-1}$ also is observed, indicating larger repeating unit

distances for the SSP2-Eu coatings. For the SSP1-Eu coatings, the sample with Si/Eu = 7/1 shows an exception. Here, a peak shift toward larger q -values is visible, which does not follow the general trend of increasing pore distance with increasing amount of europium.

The d -spacing and the size of the hexagonal domains of all coatings are summarized in Table 3. Comparing samples produced with TEOS and different amounts of the organosilane SSP1/SSP2 with samples produced with TEOS and different amounts of the europium(III)-complexed organosilane SSP1-Eu/SSP2-Eu, the former show significantly broader diffraction peaks and, thus, smaller hexagonal domains. That implies that Eu has a stabilizing effect on the mesoscopic structure.

In addition, grazing-incidence small-angle X-ray scattering (GISAXS) images were collected for selected samples to obtain more information on the pore orientation of the coatings.

Figure 4 shows GISAXS images of a calcined silicon wafer coated with a pure TEOS/surfactant sol and a silicon wafer coated with the pure SSP2-Eu with $n = 3$ (Si/Eu = 3/1). For the wafer coated with the TEOS/surfactant sol, an almost-perfect hexagonal orientation is observed with a compressed axis perpendicular to the film surface, because of shrinkage during drying. The coating prepared with the pure single-source precursor SSP2-Eu without further addition of TEOS (Si/Eu = 3/1) shows, in principle, similar features; however, the spots are strongly smeared out and appear more as a halo. This is a consequence of randomly oriented domains in the pure SSP2-Eu (Si/Eu = 3/1) sample (Figure 4B), instead of one large crystallite in the pure TEOS sample (Figure 4A). In addition, the domain size decreases from a value larger than 250 nm (which is only a given lower limit due to the resolution limit of the equipment) for pure TEOS to $\sim 60 \text{ nm}$ for the SSP2-Eu (Si/Eu = 3/1), as evaluated from the peak width by the Scherrer formula (Table 3). The domain sizes calculated from the GISAXS data coincide well with the results obtained from the transmission measurements.

The described short-range ordered or wormhole-like pore system of coatings prepared with the single-source precursor SSP2-Eu ($n = 3$) can also be observed in TEM images (see Figures 5C and 5D). Pure silica coatings with TEOS and the organosilane SSP2 result in porous materials only at low SSP2

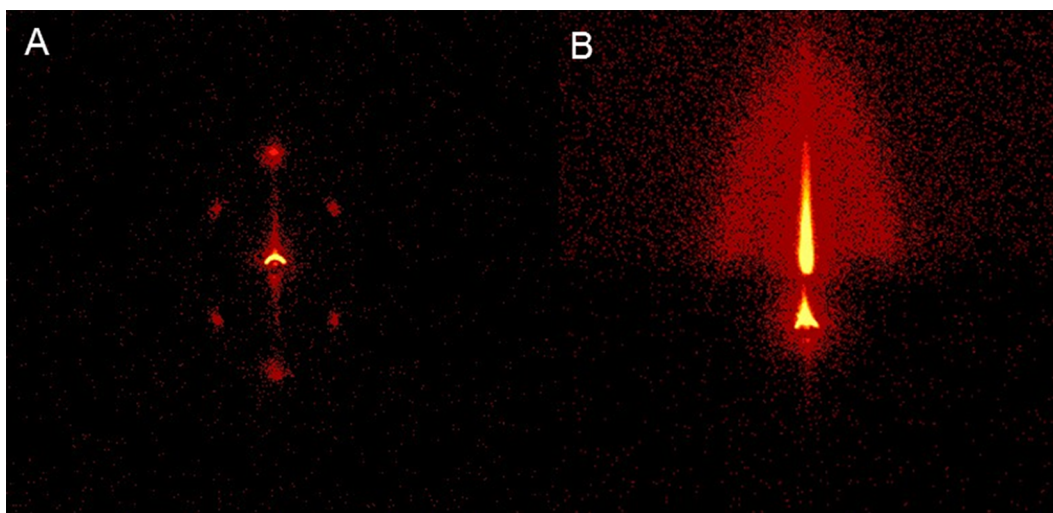


Figure 4. GISAXS pattern of (A) a pure TEOS-coated silicon wafer and (B) a wafer coated with the pure single-source precursor SSP2-Eu (Si/Eu = 3/1).

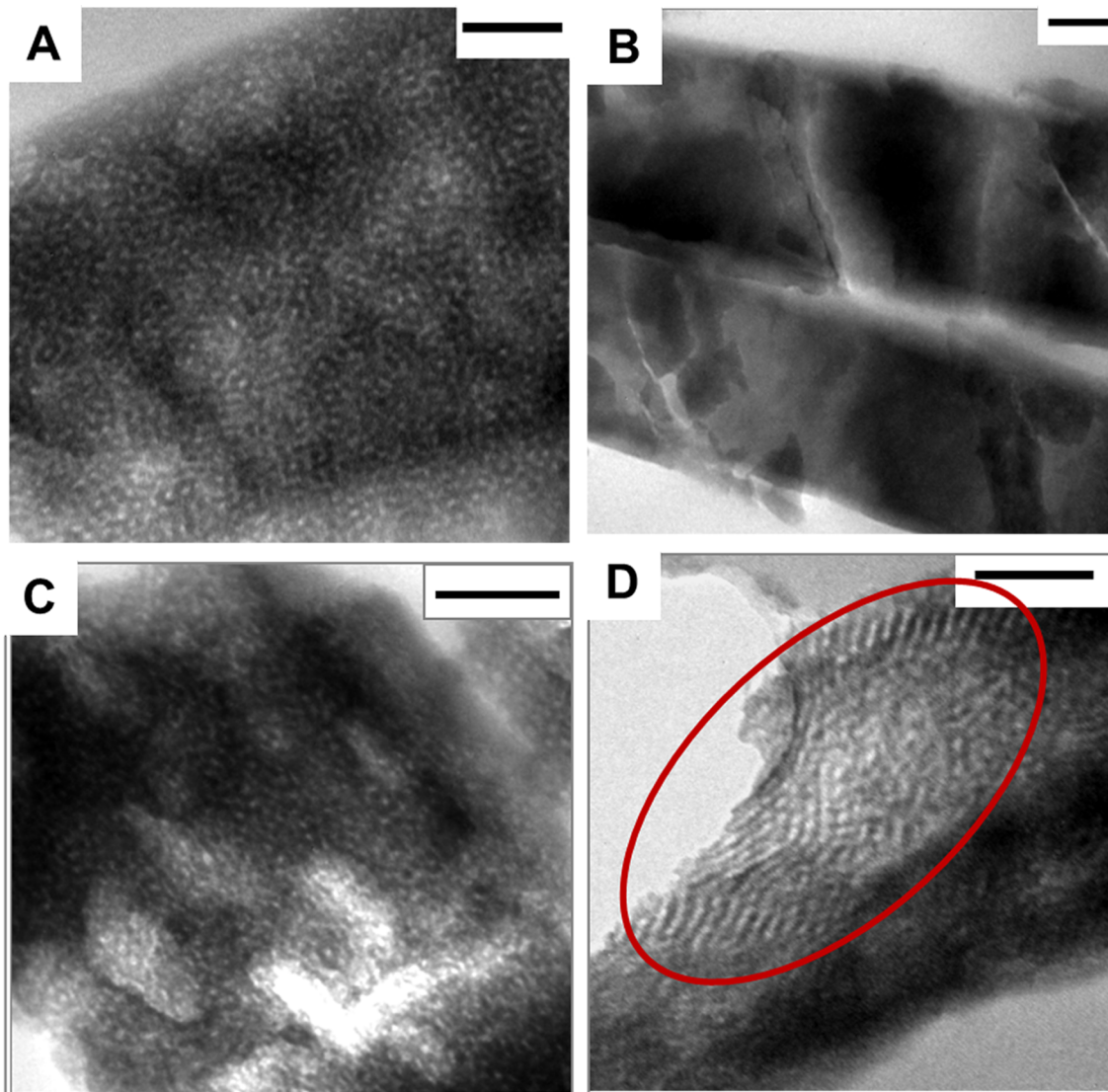


Figure 5. TEM images of coatings prepared with (A) 2.5 mol % SSP2, (B) 25.0 mol % SSP2, (C) 2.5 mol % SSP2-Eu (Si/Eu = 39/1), and (D) 12.5 mol % SSP2-Eu (Si/Eu = 7/1). The scale bars correspond to 100 nm.

concentrations (Figure 5A); higher amounts of SSP2 give nonporous materials, as seen from nitrogen sorption analysis and TEM images (Figure 5B).

The differences in porosity between the pure silica and the europium(III)-doped coatings are also reflected in the results of the nitrogen sorption measurements (Figure 6). Higher specific surface areas (S_{BET}) of the coatings could be achieved through the incorporation of europium(III) ions in the silica matrix, regardless of whether the single-source precursor SSP1-Eu or SSP2-Eu was used. Even the coated films prepared with the single-source precursors solely gave porous materials with specific surface areas of $276.1 \text{ m}^2 \text{ g}^{-1}$ for 25.0 mol % SSP1-Eu (Si/Eu = 3/1) and $178.4 \text{ m}^2 \text{ g}^{-1}$ for 25.0 mol % SSP2-Eu (Si/Eu = 3/1), respectively.

To summarize the results of the SAXS, TEM, and nitrogen sorption measurements, it can clearly be seen that the incorporation of europium(III) in the silica matrix gave porous materials in which the long-range ordering is disturbed, but small domains of hexagonally arranged mesopores are observed. The application of SSP1 and SSP2 without coordination of europium shows an even more dramatic effect on the porous

structure, with a complete loss of mesoporosity for 50 and 100 mol % SSP2. This is less pronounced when europium is coordinated to the functional organic group, and differences here can probably be related to the different hydrolysis behavior.

3.2. Dispersion of Eu³⁺ in the Silica Matrix. The surface and in-depth composition of the calcined thin films were investigated by X-ray photoelectron spectroscopy (XPS). The results for the Eu/Si ratio are in good agreement with the theoretical values across the entire film thickness. Detailed scans of the regions of interest were also acquired. Concerning the O(1s) region, a broadening of the peak was observed, thus suggesting the presence of different chemical environments for oxygen. While the O(1s) binding energy for pure silica materials is 533.1 eV, the value is shifted to 530.5 eV for pure europium(III) oxide materials.^{23,44} As can be seen in Figure 7, the values for the mixed oxide films are positioned between these two binding energies, thus indicating that Si as well as Eu atoms are located in the immediate environment of the same oxygen atom.

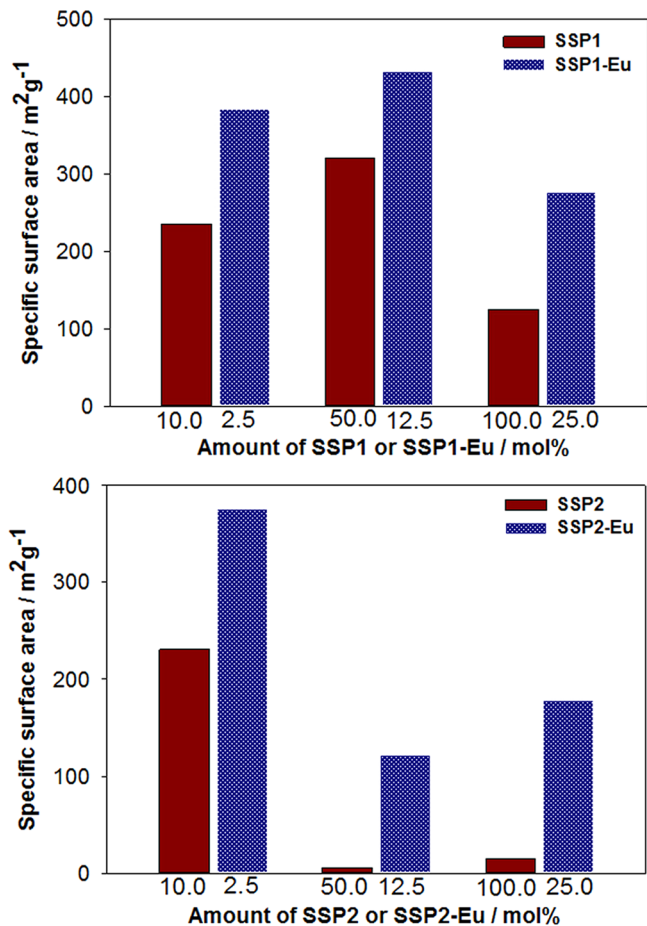


Figure 6. Specific surface areas for the powders SSP1 and SSP1-Eu (top) or SSP2 and SSP2-Eu (bottom).

3.3. Luminescence Properties. Europium(III)-doped calcined mesoporous silica films prepared with SSP1-Eu coated on silicon wafers with a molar concentration of 12.5 mol % SSP1-Eu show a red emission when irradiated by a UV lamp with an excitation energy of 254 nm (Figure 8). This observation is very remarkable because of the low thickness of the films (150–200 nm), showing the efficiency of these materials.

The respective photoluminescence emission spectra upon excitation at 280 nm are depicted in Figure 9. The five peaks located at around 580, 595, 615, 655, and 700 nm correspond to the typically observed $^5D_0 \rightarrow ^7F_J$ 4f⁶–4f⁶ transitions of Eu³⁺ with $J = 0, 1, 2, 3$, and 4, respectively. The emission band at 580 nm results from the parity-forbidden $^5D_0 \rightarrow ^7F_0$ electric dipole transition band and demonstrate, as expected, that Eu³⁺ is located in an environment with low symmetry. The emission with the highest intensity located at 605–630 nm corresponds to the $^5D_0 \rightarrow ^7F_2$ transition. Temperature-dependent measurements show an increase of the emission intensity at low temperatures, because of the higher occupation probability of excited vibrational states with increasing temperature, resulting in an increase of quenching processes. Nevertheless, characteristic emission peaks could be observed, even at room temperature. Some splitting of the emission bands can be detected at low temperatures; this will be discussed below.

The excitation spectrum shows only weak excitation peaks in the visible and near-UV region originating from the forbidden Eu f–f transitions. Small peaks can be, however, observed at

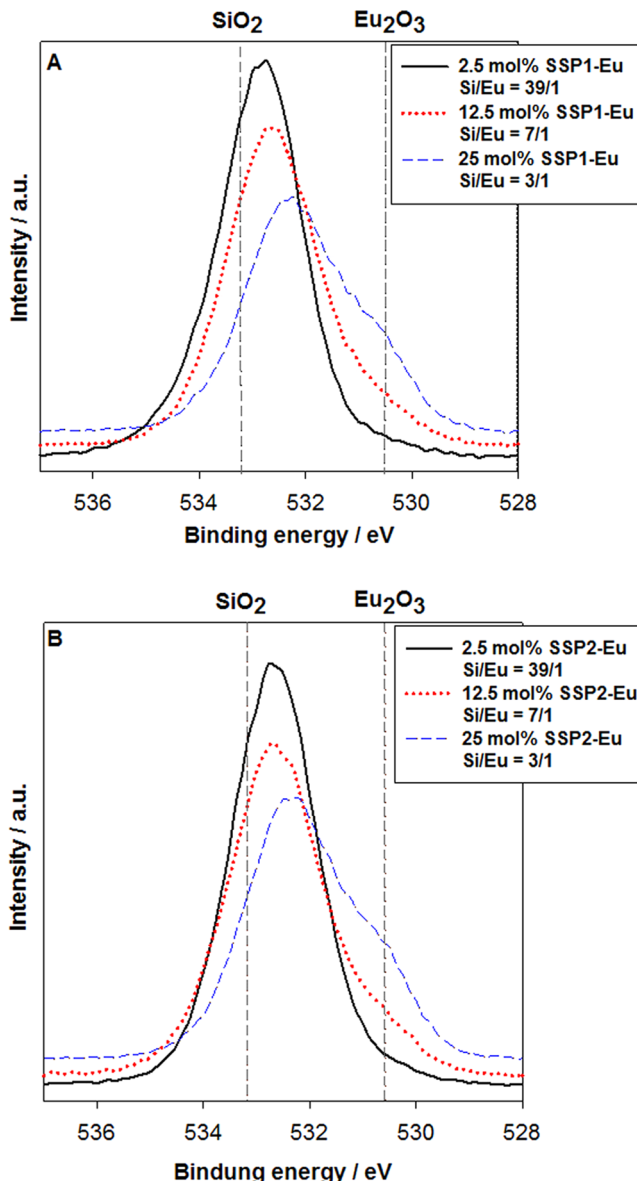


Figure 7. Binding energy of the O(1s) electron of coatings with different Eu³⁺ concentrations prepared with the single-source precursors (A) SSP1-Eu and (B) SSP2-Eu.

394 and 465 nm, respectively, which could be assigned to the $^7F_0 \rightarrow ^5L_6$ and $^7F_0 \rightarrow ^5D_2$ transition of Eu³⁺. The onset of a much more intense, broad excitation band is observed, starting at ~400 nm, originating from excitation of the silica host and Eu–O charge-transfer transitions.

Similar emission spectra could be observed for the coatings prepared via the single-source precursor SSP2-Eu. To investigate the influence of a still-higher europium concentration on the emission intensity, films were synthesized with 50 mol % SSP2-Eu. Therefore, the ratio of SSP to metal center was changed from 3:1 to 1:1 (SSP:metal). Figure 10 shows the luminescence spectra of a calcined (excitation wavelength: 270 nm) and an as-synthesized (uncalcined) (excitation wavelength: 394 nm) Eu³⁺-doped silica coating. We chose direct Eu excitation for the uncalcined samples rather than ligand excitation, because the organic ligands were decomposed after some time in the case of 270 nm excitation. The emission spectra of the uncalcined samples depict structureless broad

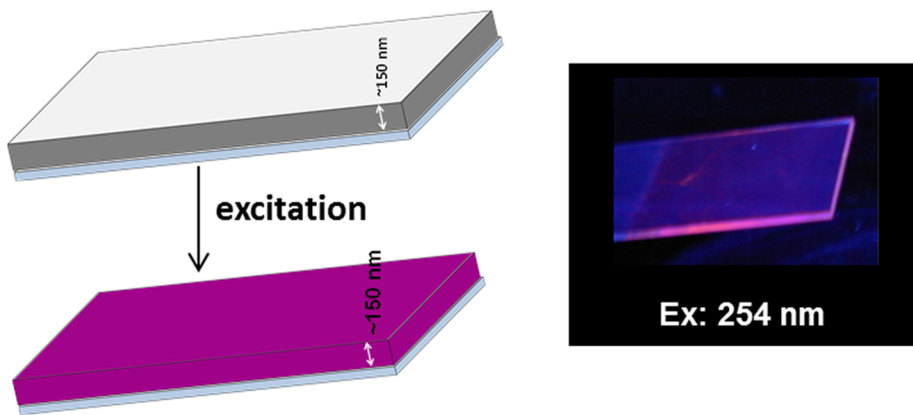


Figure 8. Red emission of a coating with a Si/Eu ratio of 7/1 (12.5 mol % SSP1-Eu).

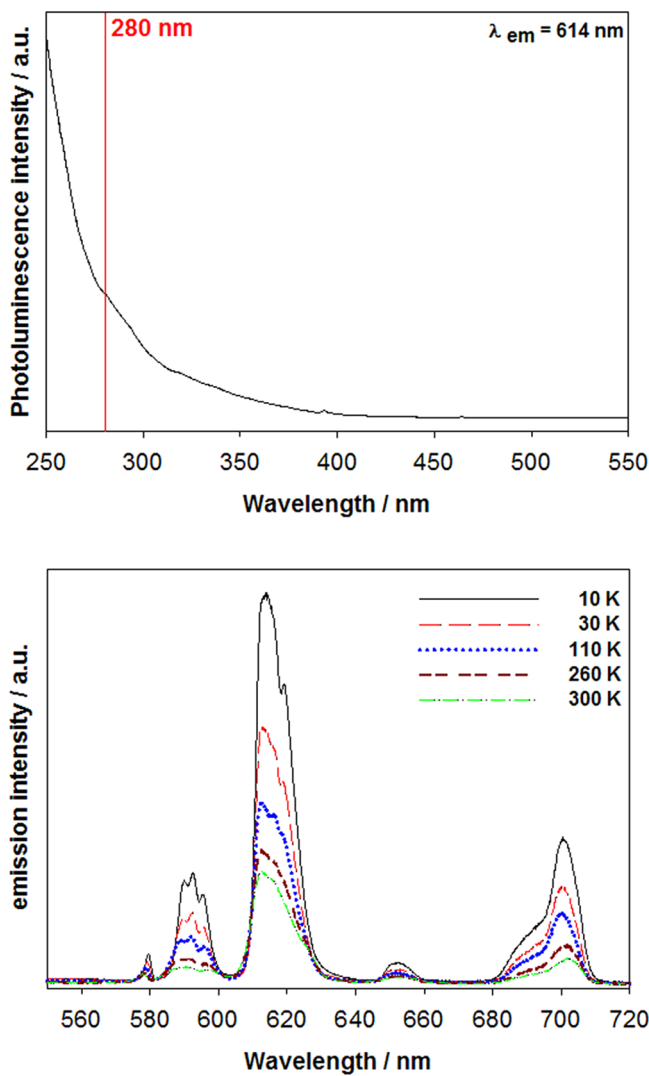


Figure 9. Excitation spectrum at room temperature (top, $\lambda_{\text{em}} = 614$ nm) and temperature-dependent emission spectra (bottom, $\lambda_{\text{ex}} = 280$ nm) of the metal oxide-doped mesoporous silica coatings doped with 12.5 mol % SSP1-Eu.

bands due to $^5D_0 \rightarrow ^7F_J$ transitions. This can be explained by the fact that numerous different coordination spheres for europium exist, which shift the crystal field levels of the 7F_J states to a small amount, so that their superimposition results in

a broad band. In contrast, in the case of calcined samples, some structure is observed for the $^5D_0 \rightarrow ^7F_2$ transitions and the width of the bands is remarkably increased. The assignment to crystal field-level splitting is rather implausible, because the width of the bands should not broaden, as in the present case. This observation may be caused by the forming of two groups of Eu sites during calcination each with comparable coordination spheres, although this point needs further investigation because the $^5D_0 \rightarrow ^7F_{0,1}$ transitions show no or almost no splitting. In general, numerous different sites should be present in such a glasslike material.

With respect to the temperature-dependent emission intensity, the properties of the calcined and the uncalcined samples differ considerably from each other. The emission intensity of the calcined coating is not detectable during these measurements (slit width 0.4 nm) at temperatures above 110 K, the emission intensity of the uncalcined samples is less temperature dependent and emission peaks can also be observed at room temperature with these settings. That means that nonradiative relaxation processes take place on a larger scale in the calcined samples than in the uncalcined one which quenches the luminescence efficiency. This behavior can be explained by the very small distance of neighboring Eu^{3+} ions after the calcination step in which the organic spacers between silicon and europium are removed. In fact, the observed concentration quenching is assumed due to the 50% concentration, and it should be emphasized that the uncalcined films show emission at room temperature, but also the calcined ones, which can be observed at lower resolutions (larger slit widths).

For further investigations, the lifetimes of the 5D_0 state of the calcined and uncalcined SSP2-Eu coatings (Si/Eu ratio = 1:1) were determined. For both samples, a biexponential decay was detected (uncalcined coatings, 0.31 and 0.39 ms; calcined coatings, 0.30 and 0.04 ms). These lifetimes are remarkably shorter than those generally observed for bulk Eu^{3+} -doped luminescent materials, which are in the range of milliseconds, but somewhat longer than that of $\text{Ni}-\text{Eu}_2\text{O}_3$ composite thin films (<0.015 ms).⁴⁵ In contrast, the doped composite film $\text{Ni}-\text{Y}_2\text{O}_3:\text{Eu}^{3+}$ has a longer lifetime of 1.04 ms, which is the same as for bulk $\text{Y}_2\text{O}_3:\text{Eu}^{3+}$.⁴⁵ Therefore, the low lifetimes of the samples presented here are due to high Eu concentrations, which lead to quenching, because of the short Eu distances mainly for the calcined samples as already observed in the emission spectra. In the case of the uncalcined samples some quenching will also be caused by high vibrational energies of

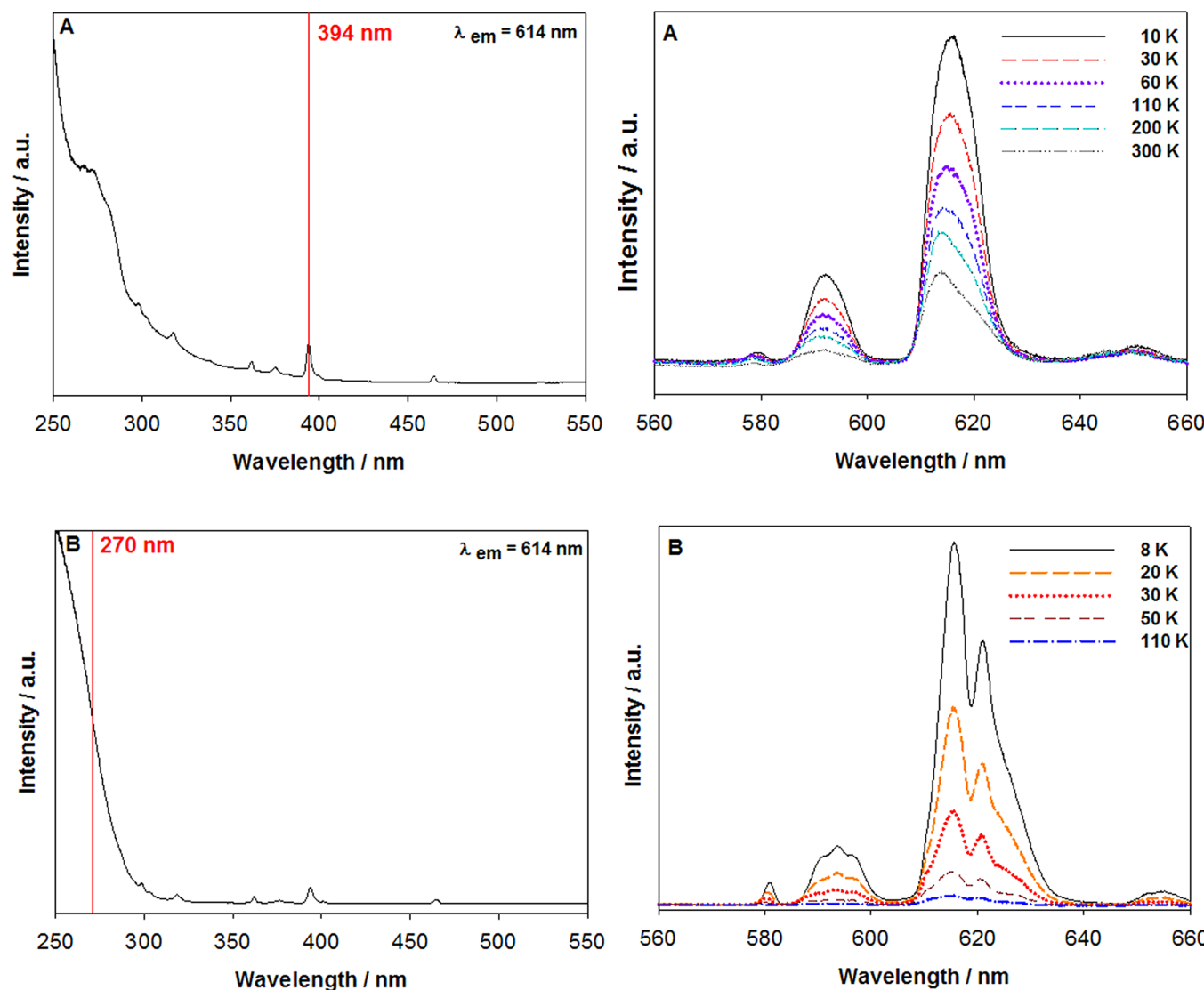


Figure 10. Excitation spectra at room temperature (left) and temperature-dependent emission spectra (right) of the coatings containing a Si/Eu ratio of 1:1 (SSP2-Eu): (A) the uncalcined coating ($\lambda_{\text{ex}} = 394 \text{ nm}$) and (B) the calcined coating ($\lambda_{\text{ex}} = 270 \text{ nm}$).

the organic linkers. The observation of biexponential decays with different lifetimes mainly for the calcined samples assists the assumption of two different types of Eu coordination.

The excitation spectrum of the calcined films is similar to those of the coatings prepared with SSP1-Eu, but some more Eu f-f transitions with higher intensity are observed in the low-energy region. The latter are also depicted for the uncalcined films, but the band due to the host has an onset at lower energy and shows some structure, which is attributed to the organic linkers.

4. CONCLUSIONS

Porous silica-europium(III) mixed metal oxide coatings on glass were successfully prepared via an evaporation-induced self-assembly process with the application of novel precursors in the presence of structure-directing agents. Deliberate substitution of the tetraethoxysilane by the functional noncoordinated trialkoxysilane already has a profound influence on the structural features of the final coatings, resulting in the most pronounced case in nonporous films, e.g., 100 mol % of SSP2. The coordination of europium(III) to the acetylacetone or

carboxylate functionality weakens this impact on the porous structure, still yielding porous coatings. However, the final europium(III)-containing silica materials show a reduced ordering of the pores in the mesoscopic range and, in parallel, the specific surface area is reduced, compared to a pure silica coating. In the case of the 5-(triethoxysilyl)pentanoic acid-modified precursor, the resulting Eu³⁺-doped silica films exhibit mesopores even at a SSP2-Eu content of 100 mol %. In addition the thin coatings show luminescence properties with characteristic emission peaks according to the $^5D_0 \rightarrow ^7F_J$ transitions. The spectra and the lifetime measurements suggests that, in the calcined materials, two different types of coordination spheres exist. The fact that the emission also is clearly visible for very thin films exhibits the efficiency of this new type of Eu-containing material.

■ AUTHOR INFORMATION

Corresponding Author

*E-mail addresses: nicola.huesing@sbg.ac.at (N.H.), wickleder@chemie.uni-siegen.de (C.W.).

Notes

The authors declare no competing financial interest.

ACKNOWLEDGMENTS

We thank Dr. T. Diemant for the XPS analyses and C. Egger for nitrogen sorption measurements. The Austrian Science Foundation FWF (Project No. I449) is acknowledged for financial support. A.F. acknowledges the financial support of the Deutsche Forschungsgemeinschaft (No. HU 1427/4-1) and the Collaborative Research Network (No. SFB 569).

REFERENCES

- (1) Pénard, A.-L.; Gacoin, T.; Boilot, J.-P. *Acc. Chem. Res.* **2007**, *40*, 895.
- (2) Juestel, T.; Nikol, H.; Ronda, C. *Angew. Chem., Int. Ed.* **1998**, *37*, 3084.
- (3) Ronda, C. R.; Juestel, T.; Nikol, H. *J. Alloys Compd.* **1998**, *275–277*, 669.
- (4) Welker, T. *J. Luminesc.* **1991**, *48&49*, 49.
- (5) Buenzli, J.-C. G.; Piguet, C. *Chem. Soc. Rev.* **2005**, *34*, 1048.
- (6) Krings, M.; Montana, G.; Dronskowski, R.; Wickleder, C. *Chem. Mater.* **2011**, *23*, 1694.
- (7) Cao, Q.-Y.; Chen, Y.-H.; Liu, J.-H.; Gao, X.-C. *Inorg. Chem. Commun.* **2009**, *12*, 48.
- (8) Wang, Y.; Yin, L.; Gedanken, A. *Ultrason. Sonochem.* **2002**, *9*, 285.
- (9) Leroy, C. M.; Wang, H. F.; Fargues, A.; Cardinal, T.; Jubera, V.; Treguer-Delapierre, M.; Boissière, C.; Grosso, D.; Sanchez, C.; Viana, B.; Pellé, F. *Phys. Chem. Chem. Phys.* **2011**, *13*, 11878.
- (10) Leroy, C. M.; Cardinal, T.; Jubera, V.; Treguer-Delapierre, M.; Majimel, J.; Manaud, J. P.; Backov, C.; Grosso, D.; Sanchez, C.; Viana, B.; Pellé, F. *ChemPhysChem* **2008**, *9*, 2077.
- (11) Reisfeld, R. *J. Fluoresc.* **2002**, *12*, 317.
- (12) Sanchez, C.; Ribot, F.; Lebeau, B. *J. Mater. Chem.* **1999**, *9*, 35.
- (13) Schubert, U.; Hüsing, N.; Lorenz, A. *Chem. Mater.* **1995**, *7*, 2010.
- (14) Lu, Q.; Wang, Z.; Wang, P.; Li, J. *Nanoscale Res. Lett.* **2010**, *5*, 761.
- (15) Lu, S. X.; Liu, Y. C. *J. Non-Cryst. Solids* **2007**, *353*, 1037.
- (16) Hui, Y. Y.; Lin, C.-F. *Mater. Lett.* **2007**, *61*, 3802.
- (17) Bruno, S. M.; Ferreira, R. A. S.; Carlos, L. D.; Pillinger, M.; Ribeiro-Claro, P.; Goncalves, I. S. *Microporous Mesoporous Mater.* **2008**, *113*, 453.
- (18) Leroy, C.; Cardinal, T.; Jubera, V.; Treguer-Delapierre, M.; Backov, R.; Boissière, C.; Grosso, D.; Sanchez, C.; Viana, B.; Pellé, F. *J. Luminesc.* **2009**, *129*, 1641.
- (19) Brinker, C. J.; Lu, Y.; Sellinger, A.; Fan, H. *Adv. Mater.* **1999**, *11*, 579.
- (20) Holland, M. A.; Pickup, D. M.; Mountjoy, G.; Tsang, E. S. C.; Wallidge, G. W.; Newport, R. J.; Smith, M. E. *J. Mater. Chem.* **2000**, *10*, 2495.
- (21) Yoldas, B. E. *J. Non-Cryst. Solids* **1980**, *38*, 81.
- (22) Pickup, B. E.; Mountjoy, G.; Wallidge, W.; Anderson, R.; Cole, J. M.; Newport, R. J.; Smith, M. E. *J. Mater. Chem.* **1999**, *9*, 1299.
- (23) Urbaniak, W.; Schubert, U. *Liebigs Ann. Chem.* **1991**, *11*, 1221.
- (24) Puchberger, M.; Rupp, W.; Bauer, U.; Schubert, U. *New J. Chem.* **2004**, *28*, 1289.
- (25) Kayan, A.; Hoebbel, D.; Schmidt, H. *J. Appl. Polym. Sci.* **2005**, *95*, 790.
- (26) Brunauer, S.; Emmett, P. H.; Teller, E. *J. Am. Chem. Soc.* **1938**, *60*, 309.
- (27) Ruland, W.; Smarsly, B. *J. Appl. Crystallogr.* **2005**, *38*, 78.
- (28) Warren, B. E. *Phys. Rev.* **1941**, *59*, 693.
- (29) Loidl, D.; Paris, O.; Burghammer, M.; Rieckel, C.; Peterlik, H. *Phys. Rev. Lett.* **2005**, *95*, 225501.
- (30) Smilgies, D. M. *J. Appl. Crystallogr.* **2009**, *42*, 1030.
- (31) Costa, V. C.; Lochhead, M. J.; Bray, K. L. *Chem. Mater.* **1996**, *8*, 783.
- (32) Meng, Q.; Boutinaud, P.; Zhang, H.; Mahiou, R. *J. Luminesc.* **2007**, *124*, 15.
- (33) Supplit, R.; Hüsing, N.; Bertagnoli, H.; Bauer, M.; Kessler, V.; Seisenbaeva, G. A.; Bernstorff, S.; Gross, S. *J. Mater. Chem.* **2006**, *16*, 4443.
- (34) Hüsing, N.; Launay, B.; Kickelbick, G.; Gross, S.; Armelao, L.; Bottaro, G.; Feth, M. P.; Kothleitner, G. *Appl. Catal., A* **2003**, *254*, 297.
- (35) Supplit, R.; Hüsing, N.; Gross, S.; Bernstorff, S.; Puchberger, M. *Eur. J. Inorg. Chem.* **2007**, *18*, 2797.
- (36) Rupp, W.; Hüsing, N.; Schubert, U. *J. Mater. Chem.* **2002**, 2594.
- (37) Böcking, D.; Fiedler, J.; Brenner, R. E.; Hüsing, N. *J. Mater. Sci.* **2009**, *44*, 6786.
- (38) Alberius, P. C. A.; Frindell, K. L.; Hayward, R. C.; Kramer, E. J.; Stucky, G. D.; Chmelka, B. F. *Chem. Mater.* **2002**, *14*, 3284.
- (39) Cagnol, F.; Grosso, D.; Sanchez, C. *Chem. Commun.* **2004**, 1742.
- (40) Nicole, L.; Boissière, C.; Grosso, D.; Quach, A.; Sanchez, C. *J. Mater. Chem.* **2005**, *15*, 3598.
- (41) Hüsing, N.; Schubert, U.; Misof, K.; Fratzl, P. *Chem. Mater.* **1998**, *10*, 3024.
- (42) Hüsing, N.; Schubert, U.; Mezei, R.; Fratzl, P.; Riegel, B.; Kiefer, W.; Kohler, D.; Mader, W. *Chem. Mater.* **1999**, *11*, 451.
- (43) Soler-Illia, G. J. A. A.; Innocenzi, P. *Chem.—Eur. J.* **2006**, *12*, 4478.
- (44) <http://srdata.nist.gov/XPS>.
- (45) Ganapathi, M.; Eliseeva, S. V.; Brooks, N. R.; Soccol, D.; Fransae, J.; Binnemans, K. *J. Mater. Chem.* **2012**, *22*, 5514.